Proceedings of the Twenty-eighth (2018) International Ocean and Polar Engineering Conference
Sapporo, Japan, June 10-15, 2018

ISBN 978-1-880653-87-6; ISSN 1098-6189

www.isope.org

Vortex Shedding and its Impacts on the Motions of a Paired-Column Semi-Submersible

Weiwen Zhao, Decheng Wan, Gang Chen
State Key Laboratory of Ocean Engineering, School of Naval Architecture, Ocean and Civil Engineering, Shanghai Jiao Tong University,
Collaborative Innovation Center for Advanced Ship and Deep-Sea Exploration, Shanghai, China

ABSTRACT

Vortex shedding of multi-column floating structures is complex due to the wake interaction between front and rear columns. The vortex shed from upstream columns will impinge upon the downstream columns and change their pressure distributions on the surface, which sequentially affects the dynamic response of vortex-induced motions (VIM). This paper tries to reveal the mechanisms of the vortex shedding, wake interference, and their impacts on the VIM of a paired-column semi-submersible by means of computational fluid dynamics (CFD). In the present work, a scaled model (1:54) of paired-column semi-submersible (PC-Semi) is studied. The CFD solver used in this paper is an in-house CFD code naoe-FOAM-SJTU, which is developed on top of the OpenFOAM framework. Turbulent flows around the geometry are modeled by delayed detached-eddy simulation (DDES). Meanwhile, the motions of the model are constrained in the horizontal plane and obtained by solving six-degrees-of-freedom motions equations. Numerical simulations at different current headings and reduced velocities are performed. The overall motion responses of the structures are evaluated. Vortex shedding process and wake impingement on downstream columns are also discussed. These preliminary results show how the vortex shedding process and wake impingement influence the VIM characteristics of a multi-column floating structures.

KEY WORDS: paired-column semi-submersible; vortex shedding; current heading; vortex-induced motions

INTRODUCTION

Vortex shedding is a common physical phenomenon on flow past bluff body. It is a consequence of boundary layer separation, which is caused by the reduction of velocity in the boundary layer, combined with a positive pressure gradient. The vortex shedding will generate periodic pressure fluctuation on alternate sides of the bluff body. For long and thin cylindrical structures, the pressure fluctuation should lead to vortex-induced vibrations (VIV). In ocean engineering, the vertical columnar shaped floating structures will suffer similar excitations, which is called vortex-induced motions (VIM). VIM is very complicated due to the involvement of flow separation, rigid body motion, mooring stiffness and other physical properties of the system. Understanding the physical principle of VIM is vital to engineers to avoid mooring line fatigue failure.

In early years, VIM studies are focused on the single column Spar platform (Dijk et al., 2003). After comprehensive studies both experimentally and numerically (Roddier et al., 2009; Lefevre et al., 2013), Spar VIM has been much better understood. However, recent studies showed that multi-column floating structures have much more complicated VIM phenomena due to the complicated vortex shedding and wake interaction among columns. Waals et al. (2007) conducted VIM model tests for semi-submersible and TLP and investigated the effects of pontoon and mass ratio to VIM response. Rijken and Leverette (2008) experimentally studied the VIM response of semi-submersible with square columns and discussed the influence of wave and external damping on VIM. Gonçalves et al. (2011a, 2012a) investigated the effects of current headings and hull appendages on a large-volume semi-submersible and confirmed the existence of vortex-induced yaw (VIY). Gonçalves et al. (2012b) subsequently studied the VIY of a semi-submersible at different current heading and draft conditions. They preferred Hilbert-Huang Transform (HHT) over Fast Fourier Transform (FFT) method for analyzing the non-stationary motion and force signals. Besides experiments, there were also some reports on VIM occurrence of full-scale semi-submersibles (Rijken and Leverette, 2009; Ma et al., 2013). It is utmost urgent to understanding the vortex shedding and wake interaction process of semi-submersibles in order to develop strategies or devices to mitigate VIM.

In the perspective of detailed flow field analyzing, the computational fluid dynamics (CFD) methods provide unparalleled advantages as it can provide the flow information of the whole computational domain. More and more researchers are involved in studying VIM of semi-submersibles using CFD. Kim et al. (2011) performed two separated simulations of a TLP model using both the finite element commercial code AcuSolve and finite volume commercial code Star-CCM+. Despite the overpredicted RMS or standard deviation of transverse motion, they concluded CFD simulations for multi-column floating body is very encouraging. Tan et al. (2013) performed a series of CFD simulation on a multi-column floating platform and discussed the modeling sensitivity such as mesh size, time-step size and different turbulence models. Lee et al. (2014) employed a Finite Analytic Navier-Stokes (FANS) code to simulate the VIM of a deep-draft semi-submersible with a wide range of current speeds and studied the scaling effect by comparing model with prototype. Chen and Chen (2016) studied different corner geometries and scale effect of a deep-draft semi-submersible by using the same FANS code.

There have already been some attempts of developing new concept deep-draft semi-submersibles to mitigate VIM. Xu (2011) proposed a new design of deep-draft semi-submersibles with blisters attached to the bottom of columns. Experimental results showed that VIM response of the new proposed design is much lower than conventional semi-submersibles. Xu et al. (2012) gave the name HVS (Heave and VIM Suppressed) to the new design and performed CFD studies on different types of blisters. On the other hand, Zou et al. (2013) performed model test on a concepted design called Paired-Column Semi-submersible (PC Semi) with a pair of columns instead of the conventional single column at four corners. They investigated the influence of current heading, gap between paired columns, the existence of inner column to VIM response. Zou et al. (2014) then carried out a series of model test with a larger model scale for PC semi. A series of subsequent CFD studies on PC Semi are conducted (Antony et al., 2015a, 2015b; Kim et al., 2015; Vinayan et al., 2015; Kara et al., 2016).

NUMERICAL OVERVIEW

Computational methodology

This paper utilizes the in-house CFD solver naoe-FOAM-SJTU to perform all the VIM simulations. The naoe-FOAM-SJTU solver is developed on top of the open source finite volume framework OpenFOAM. It is composed of six-degrees-of-freedom motion solver in combination with dynamic deforming mesh (Shen and Wan, 2013) or dynamic overset mesh (Shen et al., 2015), wave generating and absorbing module and mooring system module. As is known to all, VIM involves massively separated flow which contains strongly unsteady turbulence structures. Therefore, statistical methods such as unsteady Reynolds-Averaged Navier-Stokes (URANS) equation is not suitable for VIM prediction due to the lack information of turbulent fluctuation. The delayed detached-eddy simulation (DDES) was developed (Zhao and Wan, 2016) to accurately capture the vortex structures and has been applied to VIM simulations for deep-draft semi-submersibles (Zhao and Wan, 2017). The current DDES approach solves the $k-\omega$ SST transport equation in the near-wall flow field, and changes the turbulence length scale to a LES-like grid scale to achieve subgrid-scale (SGS) model behavior.

In general, the solution procedure can be summarized as follows. The CFD solver solves the cell-centered finite volume incompressible and viscous Navier-Stokes equations to obtain the flow field such as velocity and pressure. The turbulence kinetic energy and specific dissipate rate equation are then solved to obtain k and ω, which will be used to calculate the eddy viscosity μ_t for next timestep. The pressure and viscous shear stress are integrated over the hull surface to obtain the hydrodynamic forces and moments. Using these forces and moments, together with mooring forces and moments, the inline, transverse and yaw can be obtained.

Geometry and Conditions

In the present study, the PC Semi model with scale ratio 1:54 is chosen for VIM simulation. The corresponding model tests were performed at MARIN (Zou et al., 2014). The model was constructed with two sets of different sized columns: the larger outer columns and the smaller inner columns. Geometrical dimensions of the PC Semi are shown in Table 1 and

Fig. 1. In addition, Fig. 2 provides the three-dimensional view of the PC Semi bare hull.

Table 1. Geometrical dimensions of the PC Semi

Name	Notation (unit)	Prototype	Model
Overall width	B (m)	113.4	2.1
Draft	T (m)	53.3	0.987
Immersed column height above pontoon	H (m)	44.6	0.826
Outer column size	$L_{OC} \times W_{OC}$ (m)	13.4 × 14	0.248 × 0.259
Outer column characteristic length	D (m)	19.4	0.36
Inner column size	$L_{IC} \times W_{IC}$ (m)	10.4 × 14	0.192 × 0.259
Inner column characteristic length	d (m)	17.4	0.32
Center-to-center distance of outer column	S_{OC} (m)	96.0	1.78
Center-to-center distance of inner column	S_{IC} (m)	50.3	0.93
Pontoon height	P (m)	8.7	0.16
Pontoon width	L_p (m)	12.5	0.23

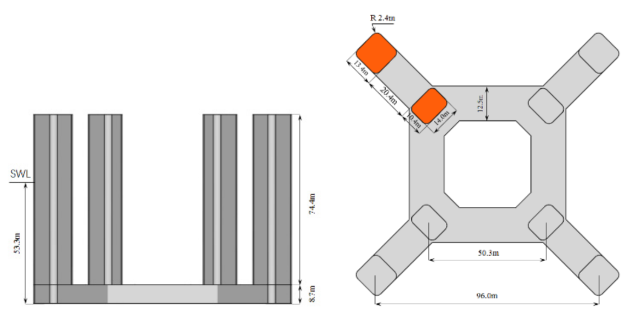

Fig. 1. Hull geometry of PC Semi prototype

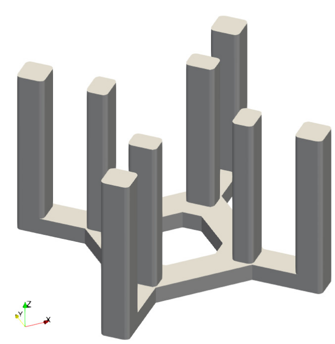

Fig. 2. Three-dimensional view of the PC Semi

The reduced velocity definition is based on the outer column diameter D

$$U_r = \frac{UT_n}{D} \tag{1}$$

Where, U and T_n are current or towing velocity and transverse natural period, respectively.

In model test, the hull model is equipped with a frictionless air bearing device on the towing carriage so that it can move freely in the horizontal plane (in-line, transverse and yaw). The current numerical study adopts the same motion constrain. The mooring system is modeled by four horizontal linear spring as shown in Fig. 3. The mass of the model is 490.2kg. The radius of gyration is 0.77593m. The effective transverse and yaw stiffness provided by the mooring system are 173.98N/m and 5.23Nm/deg, respectively. Transverse and yaw natural periods from experimental decay test are 15.45s and 9.32s. Three current headings (0, 22.5 and 45 degrees) are simulated to investigate the effects of current heading on VIM response. The current heading definition is illustrated in Fig. 4.

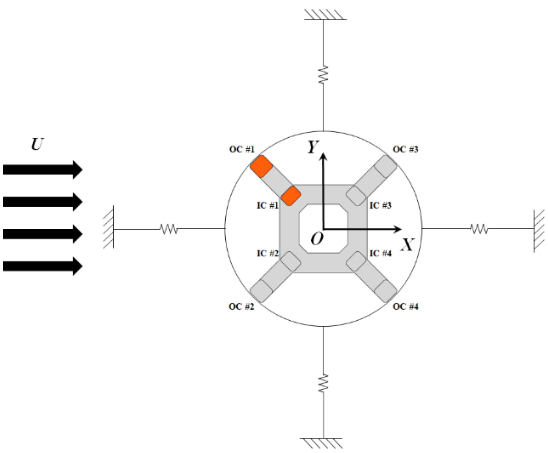

Fig. 3. Mooring configuration in current computation

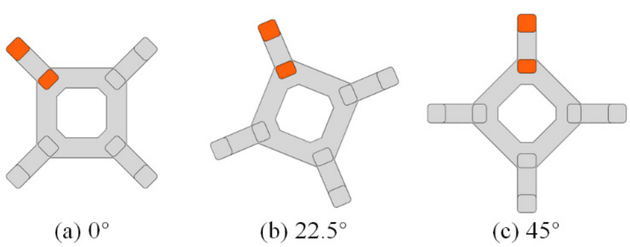

Fig. 4. Current heading definition

All simulations use a domain of $7B \times 4B \times 3.5T$ (length × width × depth) (see Fig. 5). Here, B is the overall width and T is the draft of the hull. Kim et al. (2011) used a domain of $14B \times 12B \times 4.5T$. Tan et al. (2013) adopted a $27B \times 18B \times 6T$ domain size. Meanwhile, smaller domain is also acceptable. For example, Lee et al. (2014) numerically studied VIM response of a DDS using computational domains of $6B \times 4.5B \times 2.8T$ and $5B \times 4B \times 2.2T$. Liang and Tao (2017) utilized a $9B \times 6B \times 3T$ domain in their studies of vortex shedding process of flow around a DDS. It is reasonable that the current domain is large enough to eliminate the effects from boundaries at two lateral sides, downstream and bottom.

Unstructured overset mesh is used in this study. Overset mesh consists of a set of overlapping mesh-blocks which do not share any points, edges or faces. The flow field information exchange is achieved by interpolating cell values from one mesh-block to another The naoe-FOAM-SJTU utilizes Suggar++ (Noack et al., 2009) to calculate the Domain Connectivity Information (DCIs) for interpolation. In the current study, two mesh-blocks, namely background and hull mesh are generated individually and then assembled into a whole mesh. The background mesh-block remains stationary during computation. While the hull mesh-block translates and rotates with respect to hull model.

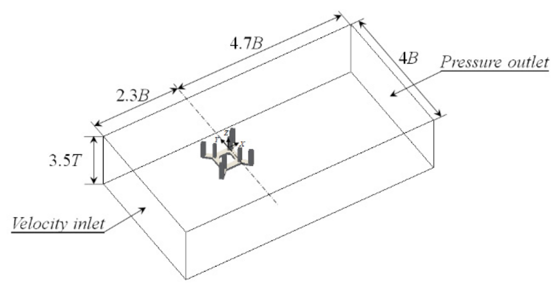

Fig. 5. Computational domain

The boundary conditions are set as follows. At inlet ($x = -2.3B$) velocity is set as $(U_c, 0, 0)$ (U_c the current velocity) and pressure is set to *zeroGradient*. At outlet ($x = 4.7B$) the velocity is set to *zeroGradient* and pressure is set to zero. Two lateral sides, bottom and top boundaries are set as symmetry plane. Note that free surface is neglected due to low Froude number condition. As for hull surface, a no-slip boundary condition is prescribed which assigns the velocity to $\boldsymbol{U}_{wall}$ and the pressure to zero normal gradient.

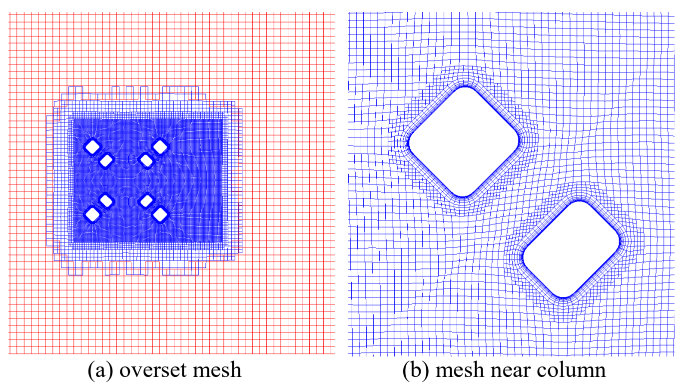

Fig. 6. Mesh for 0 degree current heading

Fig. 6 shows the grid slice at z/H=-0.5 for 0 degree current heading. Red and blue grid represent background and hull mesh-block, respectively. The background mesh takes a uniform grid. While the near hull and wake regions are refined in the hull mesh-block in order to capture the boundary layers and wake structures induced by flow separations. Four different levels of refinement zones are utilized to archive higher accuracy in critical regions. In the vicinity of columns and pontoons, 10 prism cell layers are applied to hull boundary to capture the boundary layer development. For all cases, the non-dimensioned wall distance of the first layer satisfies y+<1, which makes sure the first layer cells are located in the viscous sublayer. The total cell number is approximately 2.89 million.

The temporal derivatives in both momentum and turbulence quantities equations are discretized by second-order backward differencing scheme. A second-order upwind scheme, stabilized for transport (linear-upwind stabilized transport, LUST) is applied for convection term in momentum equation. For turbulent quantities convection terms, a second-order Total Variation Diminishing (TVD) limited linear scheme is used. The merged PISO-SIMPLE (PIMPLE) algorithm is used for pressure-velocity decoupling. PIMPLE treats every single time step as steady-state and performs SIMPLE correctors outside the PISO loop. It can run robustly at larger time step where Courant number is larger than one. The time step is set as 0.02s to ensure the Courant number is smaller than 5. Simulation time for all cases are 300s, corresponding to approximately 20 VIM cycles. All simulations are performed on a high-performance computing cluster equipped with Intel Xeon E5-2680v2 CPUs and interconnected with Infiniband FDR switches. Using 2 nodes or 40 CPU cores, the simulation can be finished within 36 hours for each case.

RESULTS AND DISCUSSIONS

Prior to VIM simulations, free decay simulation in still water is conducted to verify the natural period and effective stiffness of the preconfigured mooring system. The deviations of both transverse and yaw natural periods obtained from numerical test are within 2%, which means that the current mooring system is properly setup and can provide equivalent restore forces as the spring system used in model test. Three reduced velocities ($U_r = 5/7/9$) were computed for each current heading condition. All cases are located in the typical lock-in range.

Motion Response

To describe the non-stationary signal, the statistical nominal responses are used here. The non-dimensioned parameters are defined as

$$A_y / D = \sqrt{2}\mathrm{RMS}(y / D) \tag{2}$$

$$A_{yaw} = \sqrt{2}\mathrm{RMS}(Yaw) \tag{3}$$

Fig. 7 shows the nominal transverse and motion responses at different reduced velocities. The hollow markers represent the repeated towing tests in experiments. The filled markers are the ones obtained by current simulation. There is a huge discrepancy between the three repeated towing conditions for model tests at reduced velocity U_r=5 for 0 degree heading. Antony et al. (2015a) considered this to the instabilities of the nonlinear nature of VIM. In Kara et al. (2016), the scattered data for different runs also occurred at reduced velocity U_r=4. Kara concluded that the lock-in is a continuous process rather than fixed in one single reduced velocity. It's worth noting that the yaw response for 22.5 and 45 degrees are very close. However, in 0 degree, both transverse and yaw response is much larger than 22.5 and 45, especially at high velocity for yaw motion. A detailed explanation will be presented in the following section.

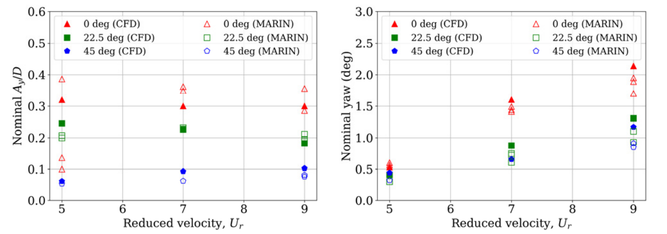

Fig. 7. Comparison of nominal transverse and yaw response between CFD and model test

Fig. 8 depicts the motion trajectories of PC Semi in horizontal plane. The shapes are similar for same current headings. At 0 degree heading, the VIM is dominated by transverse motion. In the 45 degrees heading, however, the maximum transverse motion amplitude is less than a half of 0 degree. The trajectories are irregular and gathered into a small region. It is interesting to note that at 22.5 degrees heading, the trajectory converges to a bunch of parallel lines, indicating the synchronized behavior between transverse and inline motions.

As noted by Gonçalves et al. (2011b), VIM response is non-stationary signal, which is more appropriate to be processed by the preferred Hilbert-Huang Transform (HHT) rather than Fast Fourier Transform (FFT) and wavelet analysis. HHT consists of two parts, the Empirical Mode Decomposition (EMD) and Hilbert Spectral Analysis (HSA). EMD transfers the original signal to a finite set of intrinsic mode functions (IMFs), which later will be analyzed by HSA to identify the localized features. Details for the process of EMD and HSA can be found in Huang et al. (1999). Fig. 9 shows the instantaneous frequency of transverse motion for different IMFs by HHT. The energy levels are concentrated on the first IMF (blue solid line). The frequency of IMF 1 at $U_r = 5$ is smoother and closer to natural transverse frequency (black solid line), indicating a resonance and more regular transverse motion at $U_r = 5$.

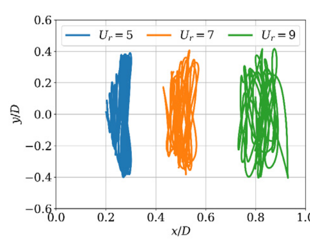

(a) 0 degree heading

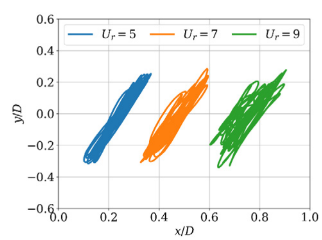

(b) 22.5 degrees heading

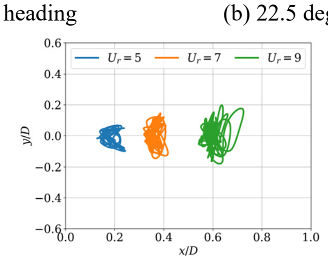

(c) 45 degrees heading

Fig. 8. Plane view of motion trajectories at different reduced velocities

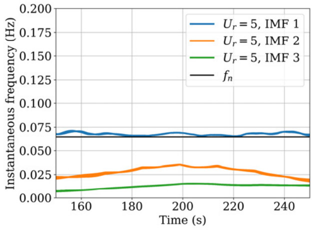

(a) $U_r = 5$, 0 degree heading

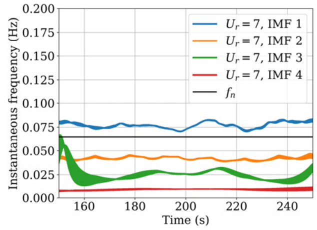

(b) $U_r = 7$, 0 degree heading

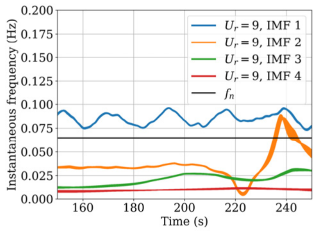

(c) $U_r = 9$, 0 degree heading

Fig. 9. Instantaneous frequency of transverse motion for different intrinsic mode functions

Instantaneous Flow Field

In order to better understanding the vortex shedding and wake interaction process between multiple columns, the flow visualizations are detailed in this section. Fig. 10 to Fig. 15 shows the non-dimensioned instantaneous vorticities $\omega_z D / U$ and the corresponding time step in motion response histories at $U_r = 7$ for all current headings. For convenience, the columns are labeled as OC#1 to OC#4 and IC#1 to IC#4 (see Fig. 3 and Fig. 4 for definition).

First take a look at 0 degree heading case (Fig. 10 and Fig. 11). When the hull is moving towards the maximum -y position (A), the vortices shed from portside of OC#1, OC#2 and IC#1, IC#2 become larger. At maximum -y position (B), the portside vortex of IC#2 first sheds and breaks into smaller vortices and impinge onto the downstream IC#4. After that, the hull moves towards positive transverse direction and leads to the starboard flow reattached onto the four upstream columns simultaneously (C). This will generate a large vortex at starboard backward position, which in consequence reduces the starboard pressure and further accelerates the hull moving towards starboard.

At 22.5 degrees heading (Fig. 12 and Fig. 13), large vortex shedding is not obvious on OC#2 and IC#2 due to the strong wake interactions between OC#2, IC#2 and IC#4. The vortex sheds from OC#2 quickly breaks into small eddies and join into IC#2's wake regions. These weak eddies directly impinge on the IC#4 and OC#4. Flow reattach still occurs in some conditions but not simultaneously, e.g., OC#2 at (B) and IC#3 at (C). This induces a phase difference of the excitation forces on difference columns, which weakens the synchronization pattern and reduces the transverse motion compared with 0 degree.

As for 45 degrees (Fig. 14 and Fig. 15), the vortices shed from upstream column OC#2 directly impinge on column IC#2 then break into smaller pieces and join with weaker vortices in the wake of IC#2. However, there are no obvious wake interactions both on the starboard and portside columns (e.g., between OC#1 and IC#1, OC#4 and IC#4) due to the side by side arrangement between the paired columns. The rectangular tail (e.g., column edge is parallel to flow) makes it difficult for flow to reattach onto the column backward. The acceleration induced by flow reattachment does not occur in this condition, which leads to a smaller transverse motion response.

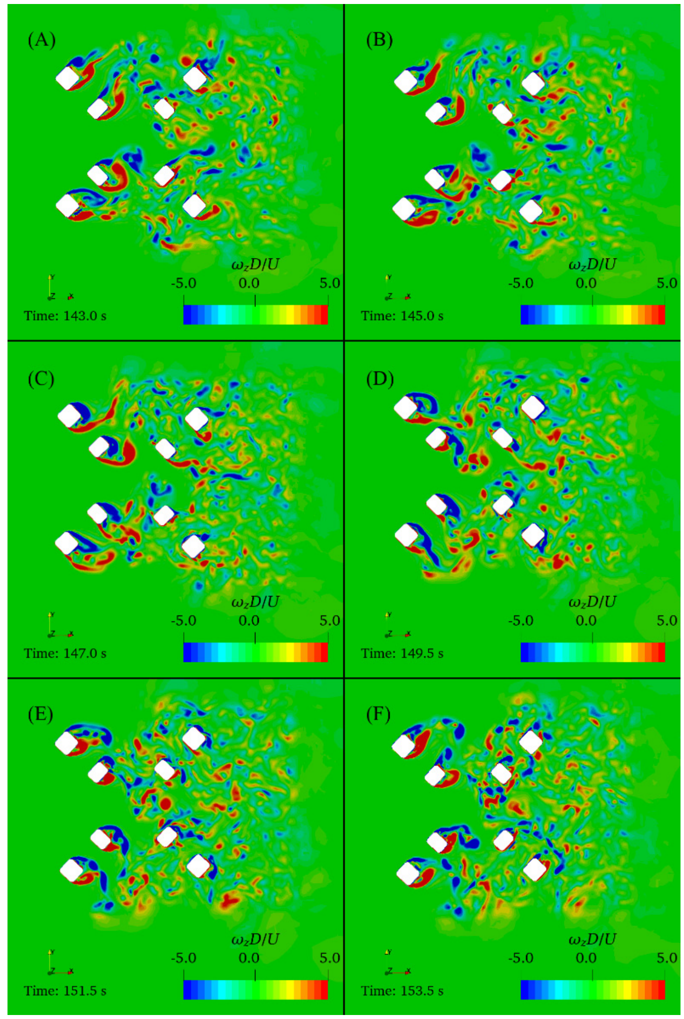

Fig. 10. Instantaneous non-dimensioned spanwise vorticity contour at half-draft plane for 0 degree heading at $U_r = 7$

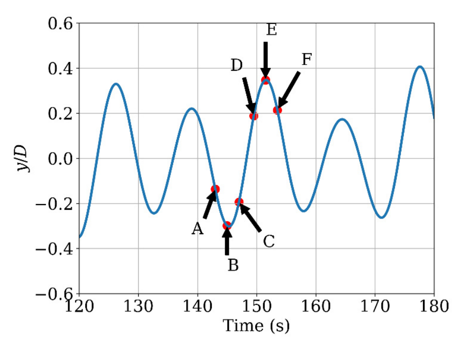

Fig. 11. Non-dimensioned transverse motion response for 0 degree heading at $U_r = 7$ with annotated time steps

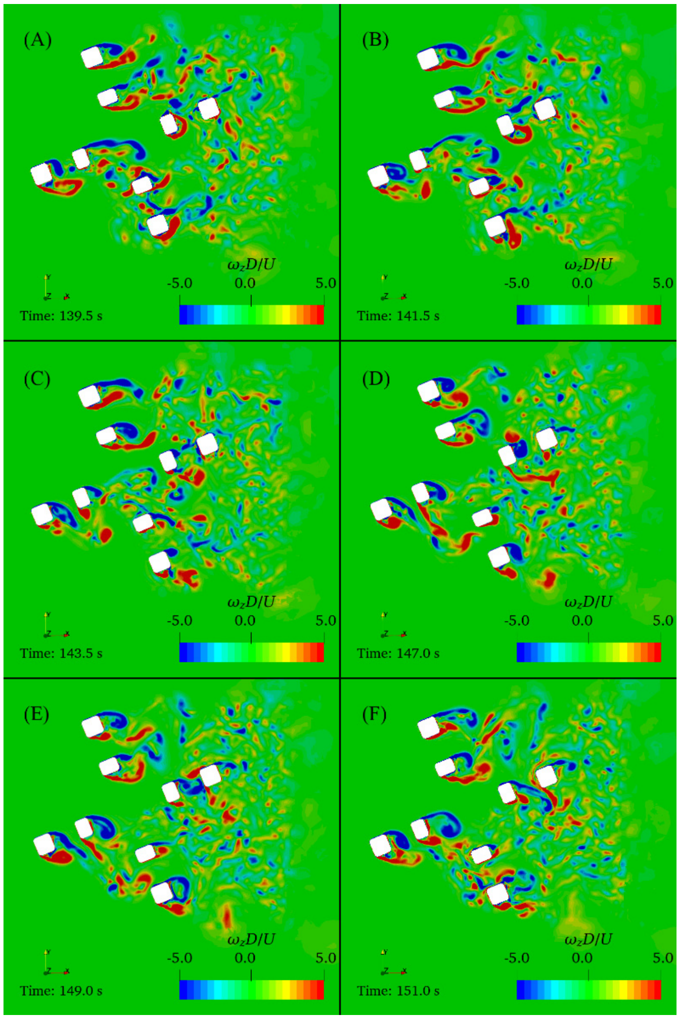

Fig. 12. Instantaneous non-dimensioned spanwise vorticity contour at half-draft plane for 22.5 degrees heading at $U_r = 7$

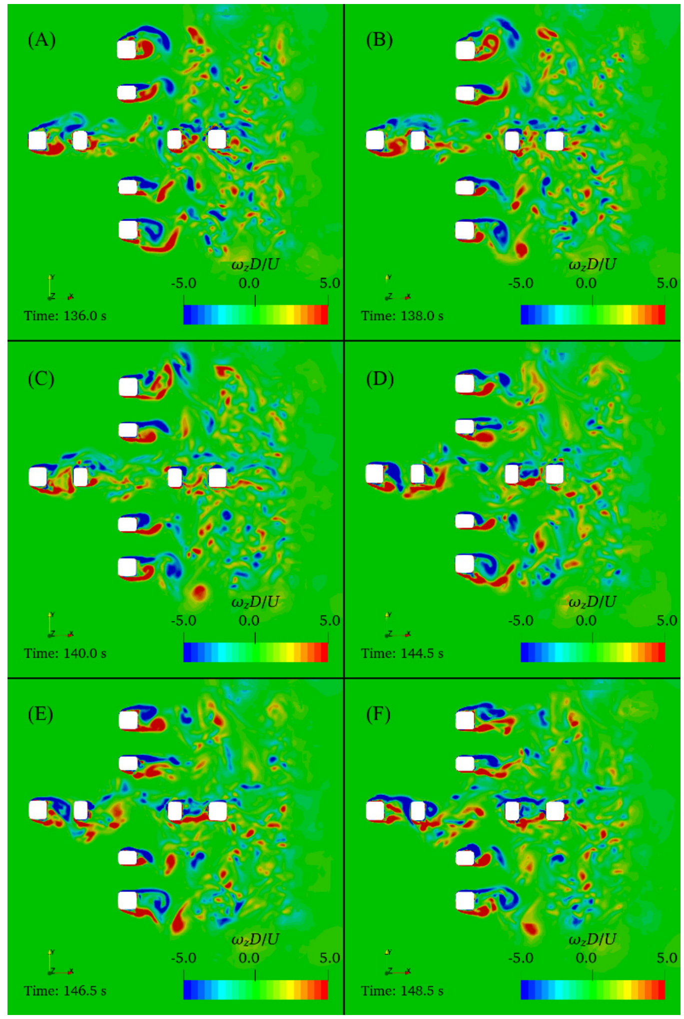

Fig. 14. Instantaneous non-dimensioned spanwise vorticity contour at half-draft plane for 45 degrees heading at $U_r = 7$

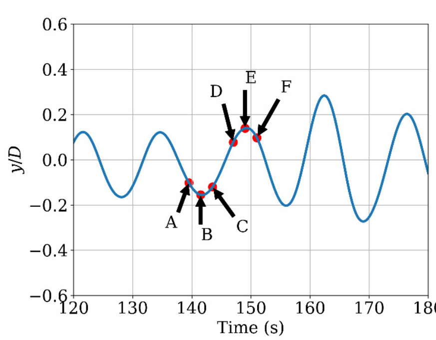

Fig. 13. Non-dimensioned transverse motion response for 22.5 degrees heading at $U_r = 7$ with annotated time steps

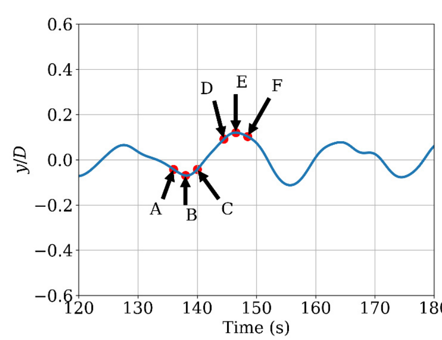

Fig. 15. Non-dimensioned transverse motion response for 45 degrees heading at $U_r = 7$ with annotated time steps

CONCLUSIONS

A series of numerical simulations of VIM on PC Semi are performed by the in-house CFD solver naoe-FOAM-SJTU. Three current headings are computed at different reduced velocities. The current predicted motion characteristics are further analyzed in both time and frequency domain. Flow visualizations are also illustrated and discussed. The following conclusions are summarized:

1. VIM responses of PC Semi are strongly directional. The shape of trajectories differs at different current headings.
2. These 0 degree cases give the largest transverse and yaw motion responses than other current headings.
3. The transverse and inline motions for 0 and 22.5 degrees heading cases are more strong and regular than 45 degrees, especially at $U_r = 5$.
4. Dominant transverse motion frequency increases as reduced velocity increases.
5. Flow reattachment after separation is more likely to occurs at 0 and 22.5 degrees.

ACKNOWLEDGEMENTS

This work is supported by the National Natural Science Foundation of China (51490675, 11432009, 51579145), Chang Jiang Scholars Program (T2014099), Shanghai Excellent Academic Leaders Program (17XD1402300), Program for Professor of Special Appointment (Eastern Scholar) at Shanghai Institutions of Higher Learning (2013022), Innovative Special Project of Numerical Tank of Ministry of Industry and Information Technology of China (2016-23/09) and Lloyd's Register Foundation for doctoral student, to which the authors are most grateful.

REFERENCES

Antony, A, Vinayan, V, Halkyard, J, Kim, S-J, Holmes, S, and Spernjak, D (2015a). "A CFD Based Analysis of the Vortex Induced Motion of Deep-Draft Semisubmersibles," *Proc Twenty-Fifth 2015 Int Ocean Polar Eng Conf*, Kona, Big Island, Hawaii, USA, 3, 1048–1055.

Antony, A, Vinayan, V, Holmes, S, Spernjak, D, Kim, SJ, and Halkyard, J (2015b). "VIM Study for Deep Draft Column Stabilized Floaters," *Offshore Technol Conf*, Houston, Texas, USA.

Chen, C-R, and Chen, H-C (2016). "Simulation of Vortex-Induced Motions of a Deep Draft Semi-Submersible in Current," *Ocean Eng*, 118, 107–116.

Dijk, RRT van, Magee, A, Perryman, S, and Gebara, J (2003). "Model Test Experience on Vortex Induced Vibrations of Truss Spars," *Offshore Technol Conf*, Houston, Texas, USA.

Gonçalves, RT, Nishimoto, K, Rosetti, GF, Fujarra, ALC, and Oliveira, AC (2011a). "Experimental Study on Vortex-Induced Motions (VIM) of a Large-Volume Semi-Submersible Platform," *Proc ASME 2011 30th Int Conf Ocean Offshore Arct Eng*, Rotterdam, The Netherlands, 7, 1–9.

Gonçalves, RT, Franzini, GR, Rosetti, GF, Fujarra, ALC, and Nishimoto, K (2011b). "Analysis Methodology for Vortex-Induced Motion (VIM) of a Monocolumn Platform Applying the Hilbert–Huang Transform Method," *J Offshore Mech Arct Eng*, 134(1), 011103.

Gonçalves, RT, Rosetti, GF, Fujarra, ALC, and Oliveira, AC (2012a). "Experimental Study on Vortex-Induced Motions of a Semi-Submersible Platform with Four Square Columns, Part I: Effects of Current Incidence Angle and Hull Appendages," *Ocean Eng*, 54, 150–169.

Gonçalves, RT, Rosetti, GF, Fujarra, C, Luís, A, Nishimoto, K, and Oliveira, C (2012b). "Vortex-Induced Yaw Motion (VIY) of a Large-Volume Semi-Submersible Platform," *Proc Twenty-Second 2012 Int Offshore Polar Eng Conf*, Rhodes, Greece, 3, 572–578.

Huang, NE, Shen, Z, and Long, SR (1999). "A New View of Nonlinear Water Waves: The Hilbert Spectrum," *Annu Rev Fluid Mech*, 31(1), 417–457.

Kara, M, Kaufmann, J, Gordon, R, Sharma, P, and Lu, J (2016). "Application of CFD for Computing VIM of Floating Structures," *Offshore Technol Conf*, Houston, Texas, USA.

Kim, J-W, Magee, A, and Guan, KYH (2011). "CFD Simulation of Flow-Induced Motions of a Multi-Column Floating Platform," *Proc ASME 2011 30th Int Conf Ocean Offshore Arct Eng*, Rotterdam, The Netherlands, 7, 319–326.

Kim, SJ, Spernjak, D, Holmes, S, Vinayan, V, and Antony, A (2015). "Vortex-Induced Motion of Floating Structures: CFD Sensitivity Considerations of Turbulence Model and Mesh Refinement," *Proc ASME 2015 34th Int Conf Ocean Offshore Arct Eng*, St. John's, Newfoundland, Canada, 2, V002T08A057.

Lee, S-K, Chien, H-P, and Gu, H (2014). "CFD Study of Deep Draft SemiSubmersible VIM," *Offshore Technol Conf-Asia*, Kuala Lumpur, Malaysia, Offshore Technology Conference.

Lefevre, C, Constantinides, Y, Kim, JW, Henneke, M, Gordon, R, Jang, H, and Wu, G (2013). "Guidelines for CFD Simulations of Spar VIM," *Proc 32nd Int Conf Offshore Mech Arct Eng - OMAE*, Nantes, France, 7, V007T08A019.

Liang, Y, and Tao, L (2017). "Interaction of Vortex Shedding Processes on Flow over a Deep-Draft Semi-Submersible," *Ocean Eng*, 141, 427–449.

Ma, W, Wu, G, Thompson, H, Prislin, I, and Maroju, S (2013). "Vortex Induced Motions of a Column Stabilized Floater," *Proc DOT Int Conf*, Houston, Texas, USA.

Noack, RW, Boger, DA, Kunz, RF, and Carrica, PM (2009). "Suggar++: An Improved General Overset Grid Assembly Capability," *19th AIAA Comput Fluid Dyn Conf*, San Antonio, Texas, USA.

Rijken, O, and Leverette, S (2008). "Experimental Study into Vortex Induced Motion Response of Semi Submersibles with Square Columns," *Proc ASME 27th Int Conf Offshore Mech Arct Eng*, Estoril, Portugal, 1, 263–276.

Rijken, O, and Leverette, S (2009). "Field Measurements of Vortex Induced Motions of a Deep Draft Semisubmersible," *Proc ASME 28th Int Conf Ocean Offshore Arct Eng*, Honolulu, Hawaii, USA, 6, 739–746.

Roddier, D, Finnigan, T, and Liapis, S (2009). "Influence of the Reynolds Number on Spar Vortex Induced Motions (VIM): Multiple Scale Model Test Comparisons," *Proc ASME 28th Int Conf Ocean Offshore Arct Eng*, Honolulu, Hawaii, USA, 5, 797–806.

Shen, Z, and Wan, DC (2013). "RANS Computations of Added Resistance and Motions of a Ship in Head Waves," *Int J Offshore Polar Eng*, 23(4), 263–271.

Shen, Z, Wan, DC, and Carrica, PM (2015). "Dynamic Overset Grids in OpenFOAM with Application to KCS Self-Propulsion and Maneuvering," *Ocean Eng*, 108, 287–306.

Tan, JHC, Magee, A, Kim, JW, Teng, YJ, and Zukni, NA (2013). "CFD Simulation for Vortex Induced Motions of a Multi-Column Floating Platform," *Proc ASME 2013 32nd Int Conf Ocean Offshore Arct Eng*, Nantes, France, 7, V007T08A066.

Vinayan, V, Antony, A, Halkyard, J, Kim, S-J, Holmes, S, and Spernjak, D (2015). "Vortex-Induced Motion of Deep-Draft Semisubmersibles: A CFD-Based Parametric Study," *Proc ASME 2015 34th Int Conf Ocean Offshore Arct Eng*, St. John's, Newfoundland, Canada, 2, V002T08A003.

Waals, OJ, Phadke, AC, and Bultema, S (2007). "Flow Induced Motions of Multi Column Floaters," *Proc 26th Int Conf Offshore Mech Arct Eng*, San Diego, California, USA, 1, 669–678.

Xu, Q (2011). "A New Semisubmersible Design for Improved Heave Motion, Vortex-Induced Motion and Quayside Stability," *Proc ASME 2011 30th Int Conf Ocean Offshore Arct Eng*, Rotterdam, The Netherlands, 7, 95–103.

Xu, Q, Kim, J, Bhaumik, T, O'Sullivan, J, and Ermon, J (2012). "Validation of HVS Semisubmersible VIM Performance by Model Test and CFD," *Proc ASME 2012 31st Int Conf Ocean Offshore Arct Eng*, Rio de Janeiro, Brazil, 1, 175–185.

Zhao, W, and Wan, DC (2016). "Detached-Eddy Simulation of Flow Past Tandem Cylinders," *Appl Math Mech*, 37(12), 1272–1281.

Zhao, W, and Wan, DC (2017). "CFD Study of VIM of a Paired-Column Semi-Submersible Platform," *Proc Twenty-Seventh 2017 Int Ocean Polar Eng Conf*, San Francisco, California, USA, International Society of Offshore and Polar Engineers, 3, 693–700.

Zou, J, Poll, P, Roddier, D, Tom, N, and Peiffer, A (2013). "VIM Testing of a Paired Column Semi Submersible," *Proc ASME 2013 32nd Int Conf Ocean Offshore Arct Eng*, Nantes, France, 7, V007T08A001.

Zou, J, Poll, P, Antony, A, Das, S, Padmanabhan, R, Vinayan, V, and Parambath, A (2014). "VIM Model Testing and VIM Induced Mooring Fatigue of a Dry Paired-Column Semisubmersible Platform," *Offshore Technol Conf*, Houston, Texas, USA.